Anisotropy in Broken Cloud Fields Over Oklahoma from Landsat Data

L. M. Hinkelman
National Institute of Aerospace
Hampton, Virginia

K. F. Evans
University of Colorado
Boulder, Colorado

Introduction

Previously, it was shown (Hinkelman et al. 2002) that anisotropy, or the existence of a preferred direction, in cumulus fields significantly affects solar radiative transfer through these fields. In this poster, we investigate the occurrence of anisotropy in broken cloud fields near the Atmospheric Radiation Measurement (ARM) Program Southern Great Plains (SGP) site imaged by the Landsat 7 enhanced thematic mapper (ETM).

Method

Sample Landsat scenes of cumuloform clouds with different types of organization over Central Oklahoma, including the ARM Cloud and Radiation Testbed site to the northeast, were obtained from the National Aeronautics and Space Administration (NASA) earth observing plan (EOS) DataGateway. (Only four scenes were used because of the high cost of this data.) For each scene, the range of colors characteristic of the clouds was identified by eye and a cloud mask was created by selecting the pixels within this range using Adobe Photoshop tools.

The anisotropy parameter was calculated over a range of scales for several 25.6 x 25.6 km^2 regions from each cloud mask. This parameter indicates the strength and direction of orientation at each given scale. The anisotropy parameter A is calculated for a two-dimensional field in the Fourier domain according to

$$|A_n| = \frac{\sqrt{M_{c,n}^2 + M_{s,n}^2}}{M_{0,n}}; \angle(A_n) \equiv \frac{1}{2} tan^{-1}\left(\frac{M_{s,n}}{M_{c,n}}\right)$$

where

$$M_{0,n} = \int_{k_{n-1}}^{k_n} \int_0^{2\pi} S(k,\phi) d\phi\, dk$$

$$M_{c,n} = \int_{k_{n-1}}^{k_n} \int_0^{2\pi} S(k,\phi) cos(2\phi) d\phi\, dk$$

$$M_{s,n} = \int_{k_{n-1}}^{k_n} \int_0^{2\pi} S(k,\phi) sin(2\phi) d\phi\, dk$$

Here *S* is the power spectrum of the field, *n* is the spatial frequency band index, and *s* and *c* indicate the sine and cosine terms, respectively. Figure 1, which shows a sample power spectrum in frequency space marked with octave spatial frequency bins, illustrates the geometry of this calculation. Because the Landsat data was not periodic, a cosine taper was applied to the outer 6 km of data on each edge of the cloud masks before the Fourier transform was taken.

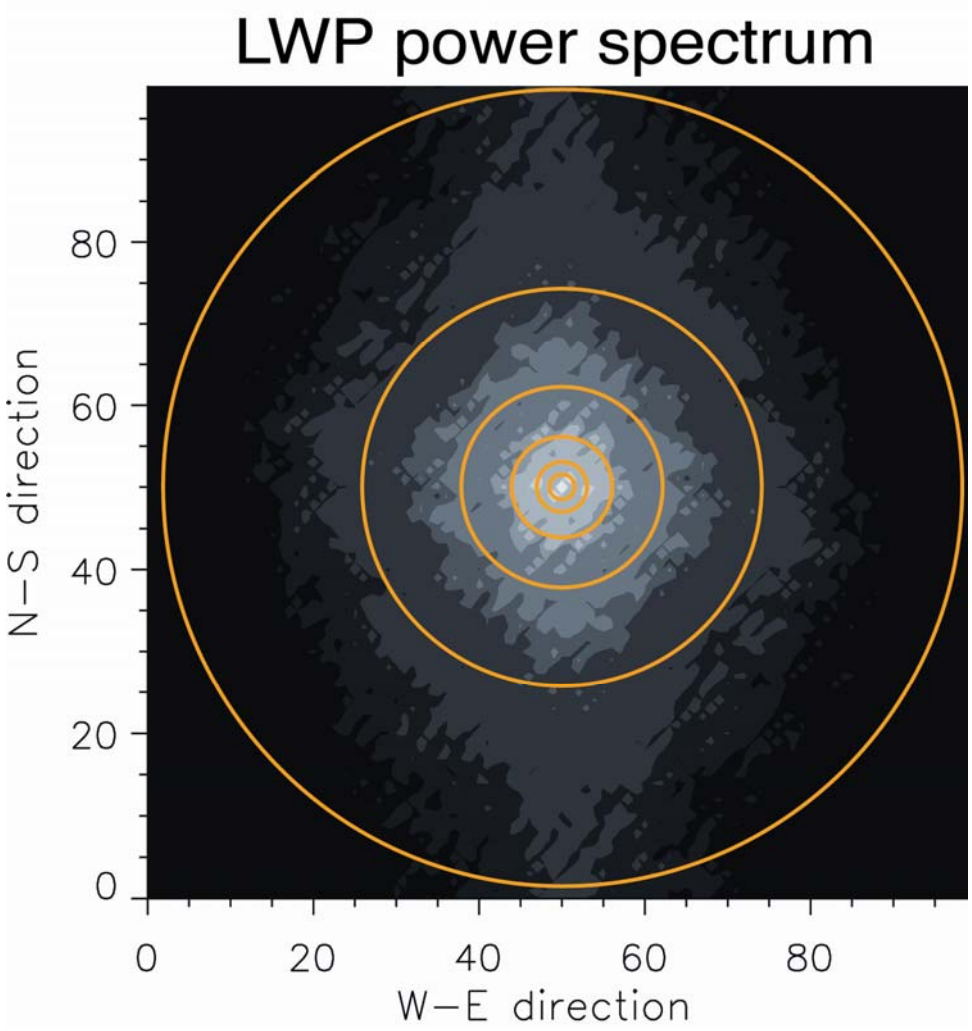

Figure 1. Geometry of the anisotropy parameter calculation.

The probability of a given anisotropy parameter amplitude occurring by chance varies with the number of points in the spatial frequency band. In order to normalize the results, 95% significance values were calculated for all spatial frequency bands using a Monte Carlo technique. Five-thousand stochastic and nominally isotropic fields were calculated by filtering arrays of Gaussian random values in the frequency domain, Fourier transforming them back to the real domain, and thresholding the results to give binary "cloud masks" with the desired range of cloud fractions. The filter was designed so that the power spectrum of the binary fields matched that average spectrum of the Landsat region cloud masks.

In our previous work using three-dimensional cloud fields (Hinkelman et al. 2004) we were able to distinguish between orientation due to horizontal stretching and orientation due vertical cloud tilt. Although in these scenes shadows give some suggestion of cloud surface topography, the two-dimensional nature of the images prevents independent detection of stretching and tilt.

Since our study (Hinkelman et al. 2004) of large-eddy simulation output at scales below 2 km showed that anisotropy is often associated with vertical wind shear and high wind velocities, we compared the anisotropy results to wind data. Rapid update cycle (RUC) analysis data for the time of the Landsat overflight (~17 Universal Time Coordinates [UTC]) was obtained from the ARM archive. The heights containing clouds were determined from the RUC relative humidity profiles and active remote sensing cloud layer plots. Vertical shears were computed from the wind data provided and then both shears and winds were averaged over the cloudy levels for RUC grid points within the Landsat field of view. The mean winds and shears over this area were also calculated.

Results and Discussion

For each Landsat scene, the following information is presented:

- A false-color overview image of the scene on which the regions for which anisotropy has been calculated are marked. The SGP site central facility is near the top of the image, toward the right (East).

- An enlarged cloud mask image for one region of particular interest.

- Anisotropy parameter vectors normalized by the 95% significance values plotted as a function of scale for all selected regions. The vectors having amplitudes greater than the appropriate significance values are highlighted in red.

- Wind and shear fields over the Landsat image area.

Area mean wind (dark blue) and shear (cyan) vectors accompany the false-color scene images. All wind speeds are given in ms^{-1}; shears are in $ms^{-1}km^{-1}$.

July 7, 1999 (Figures 2 to 5)

The clouds in this scene appear to be arranged relatively randomly, but significant anisotropy is detected at moderate and small scales in most regions. This anisotropy is oriented close to the direction of the average wind shear.

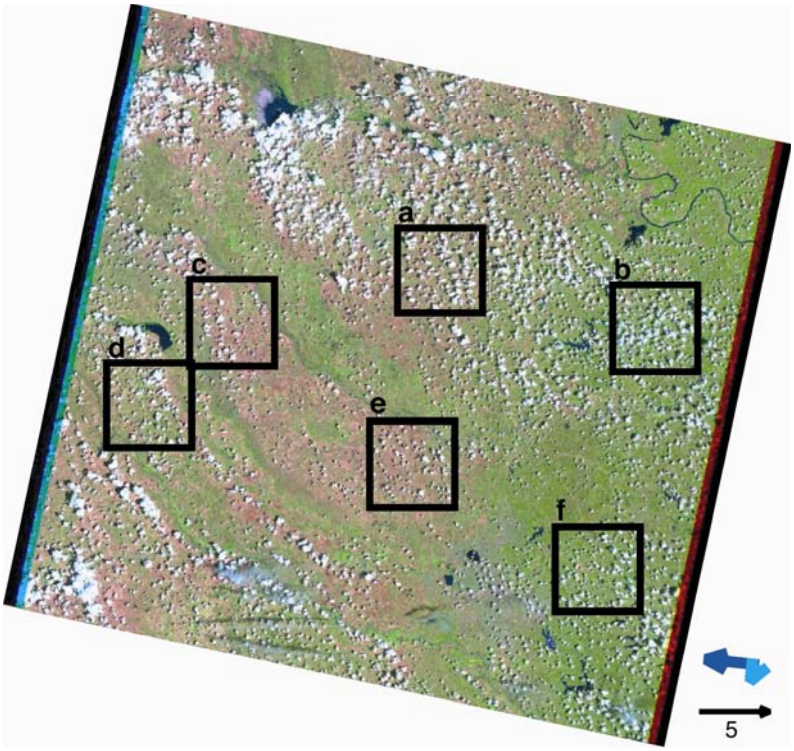

Figure 2. False-color Landsat ETM scene over central Oklahoma for July 7, 1999, showing fair-weather cumulus clouds.

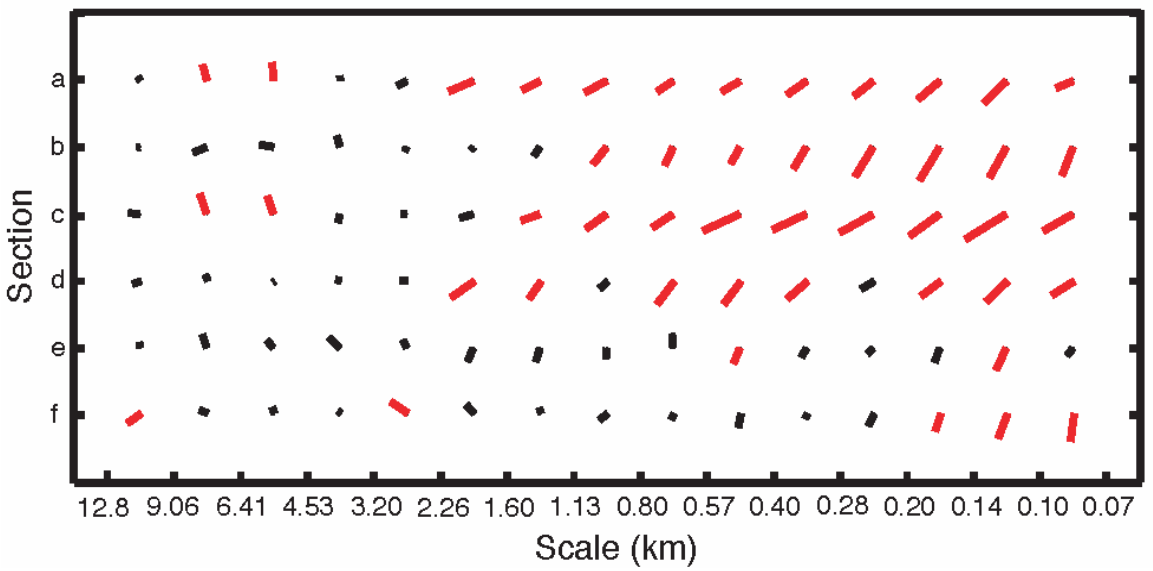

Figure 3. Anisotropy parameter vectors for the six regions marked in Figure 2.

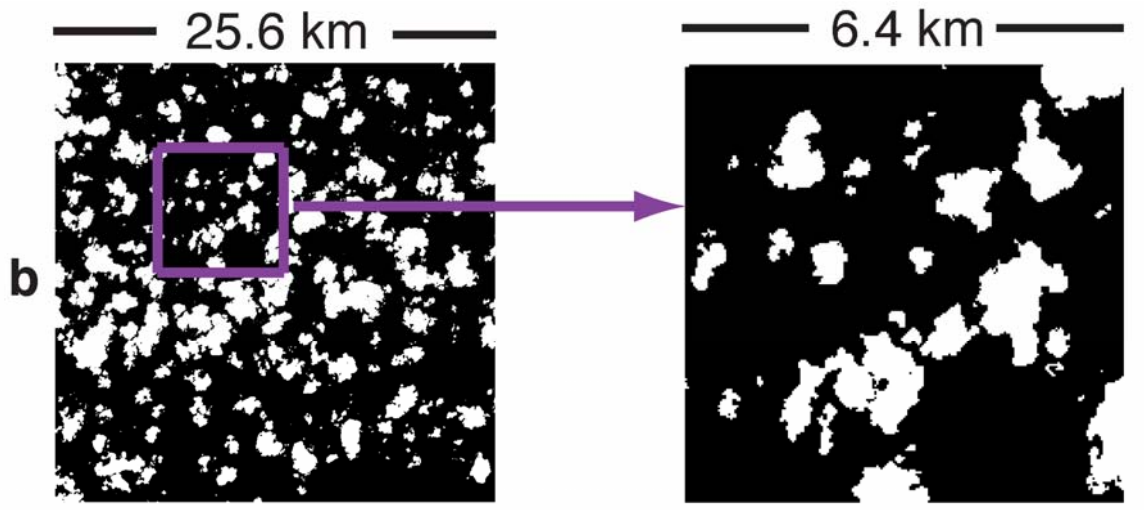

Figure 4. Enlargements of the cloud mask for region b in Figure 2. Although at the larger scales the clouds appear randomly oriented, SW-NE alignment is apparent at small scales.

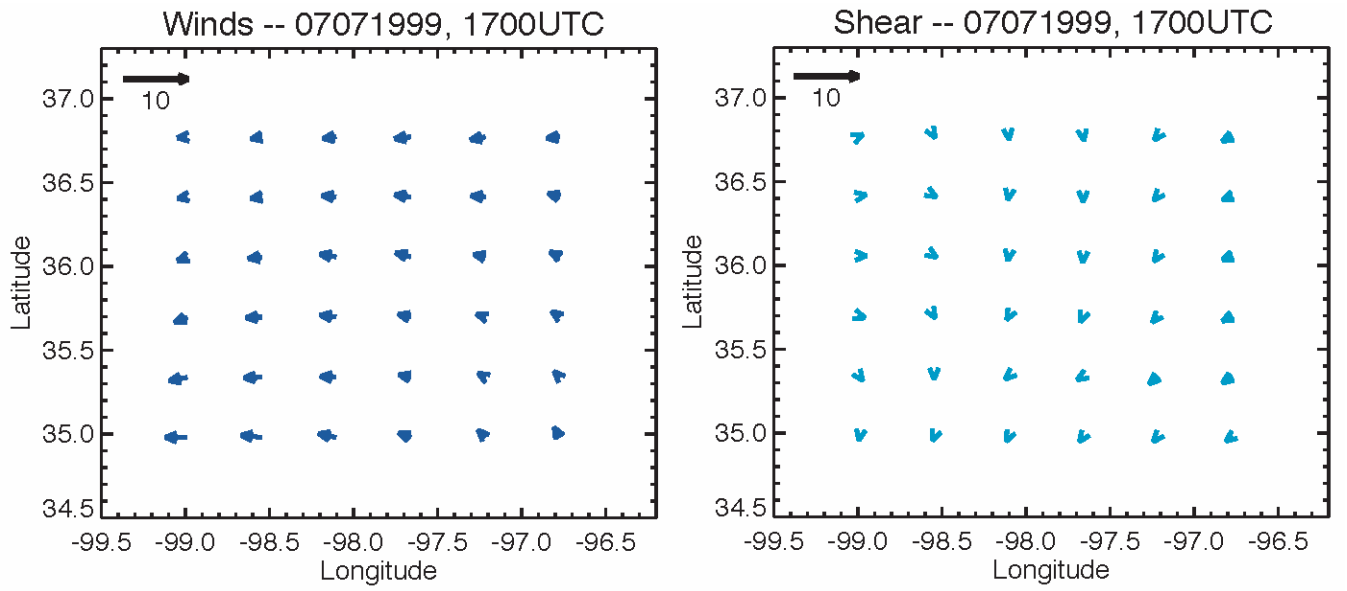

Figure 5. Wind and shear fields for the entire Landsat scene at 1700 UTC on July 7, 1999.

September 25, 1999 (Figures 6 to 9)

Changes in the direction of large-scale organization stand out in this image and seem to correlate with changes in the wind direction. Except in the higher cloud fraction region f, anisotropy at the smaller scales is generally nearly perpendicular to the large-scale structure. Some correlation with shear is evident in the cloud orientation at small-scales.

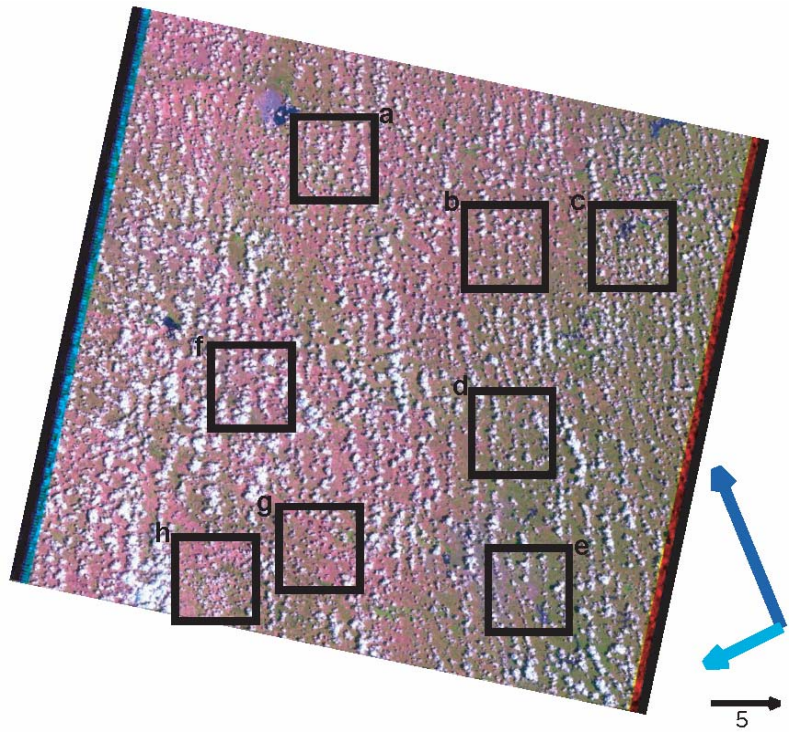

Figure 6. False-color Landsat ETM scene over central Oklahoma for September 25, 1999, showing a stratoculmulus deck transitioning to broken cumulus clouds.

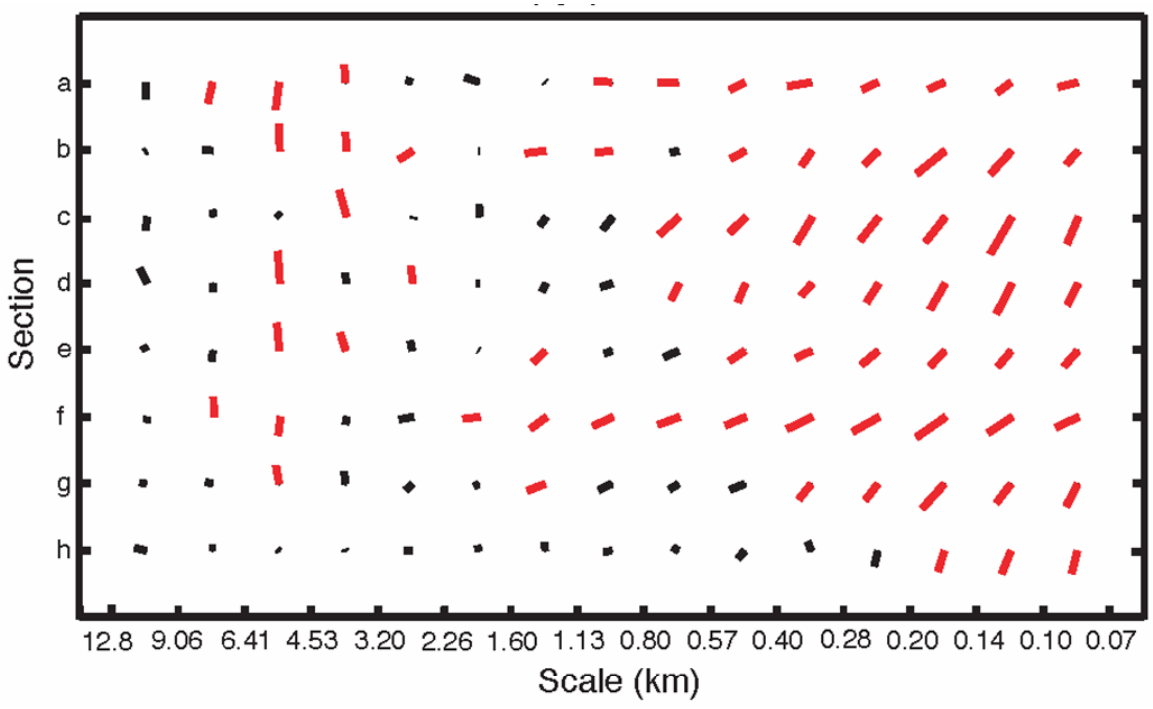

Figure 7. Anisotropy parameter vectors for the six regions marked in Figure 6.

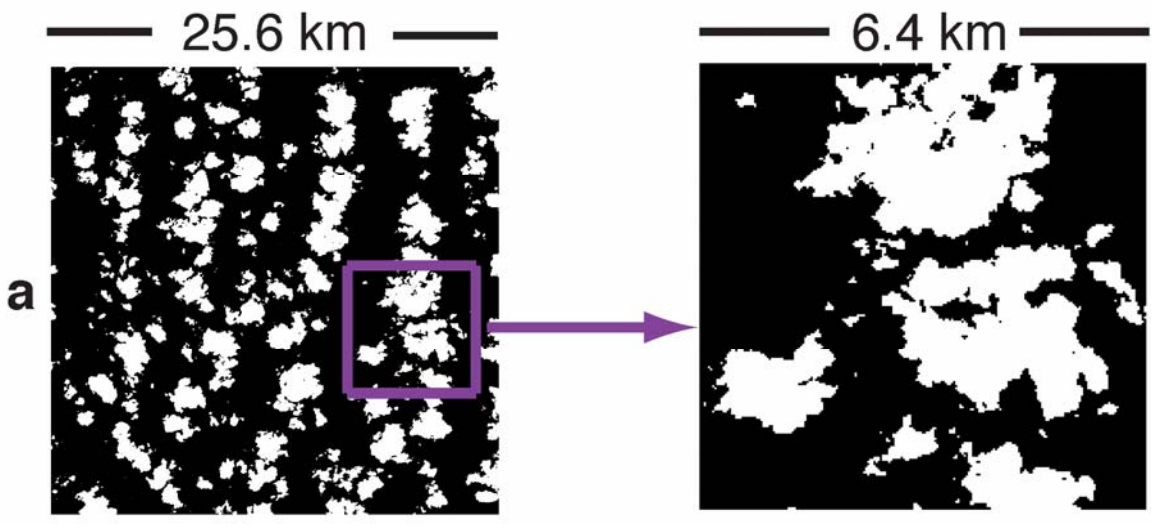

Figure 8. Enlargements of the cloud mask for region a in Figure 6. Individual cloud cells are stretched along the southwest-northeast diagonal, perpendicular to the large-scale orientation axis.

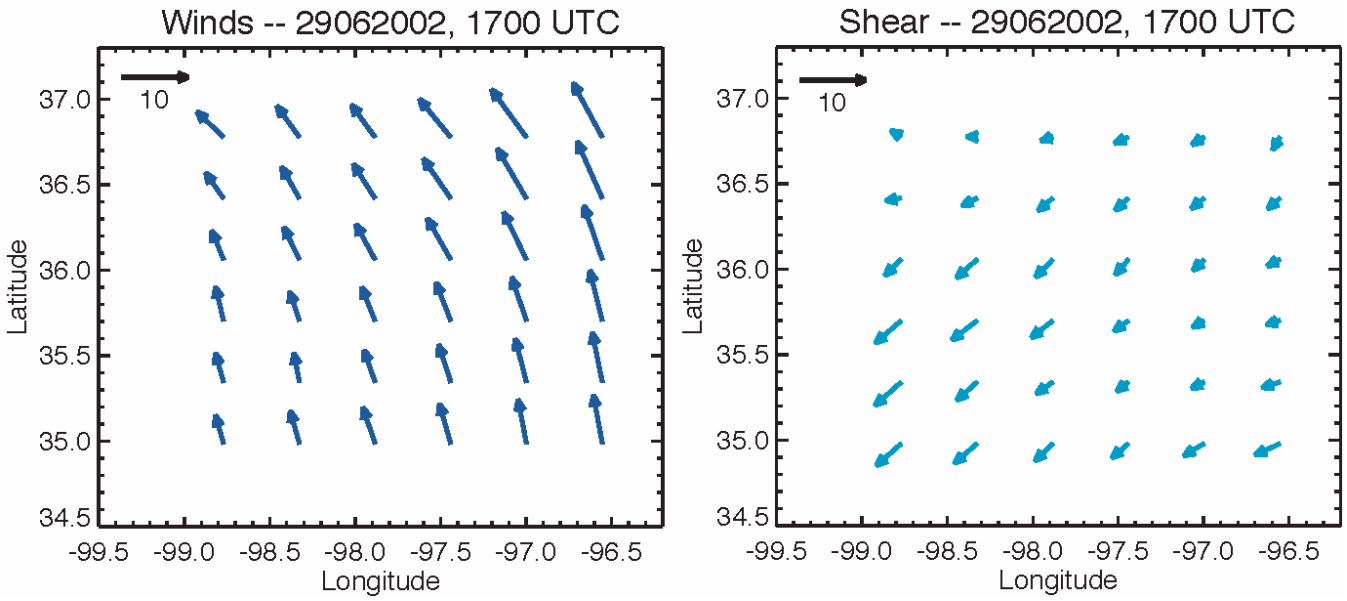

Figure 9. Wind and shear fields for the entire Landsat scene at 1700 UTC on June 29, 2002.

June 29, 2002 (Figures 10 to 13)

The ragged cloud streets in this image are detected at scales close to their wavelength (~4-6 km). While the cloud streets are oriented just to the right of the wind direction, the individual cloud cells tend to align with the shear direction. Note that the roll structure is not continuous over the whole scene – more random patches occur in regions g and h, for example.

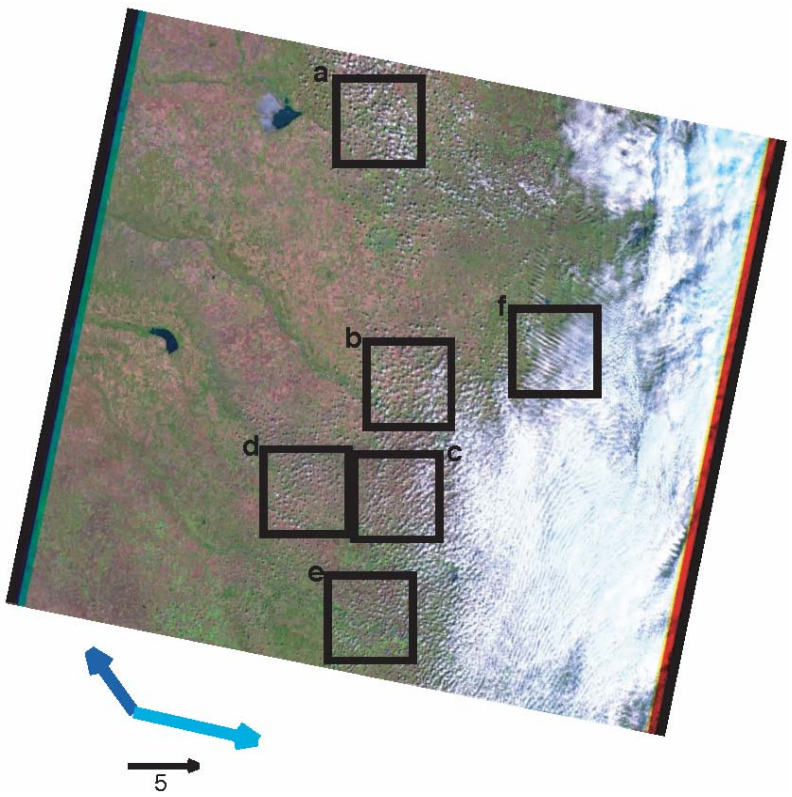

Figure 10. False-color Landsat ETM scene over central Oklahoma for June 29, 2002, showing ragged cloud streets.

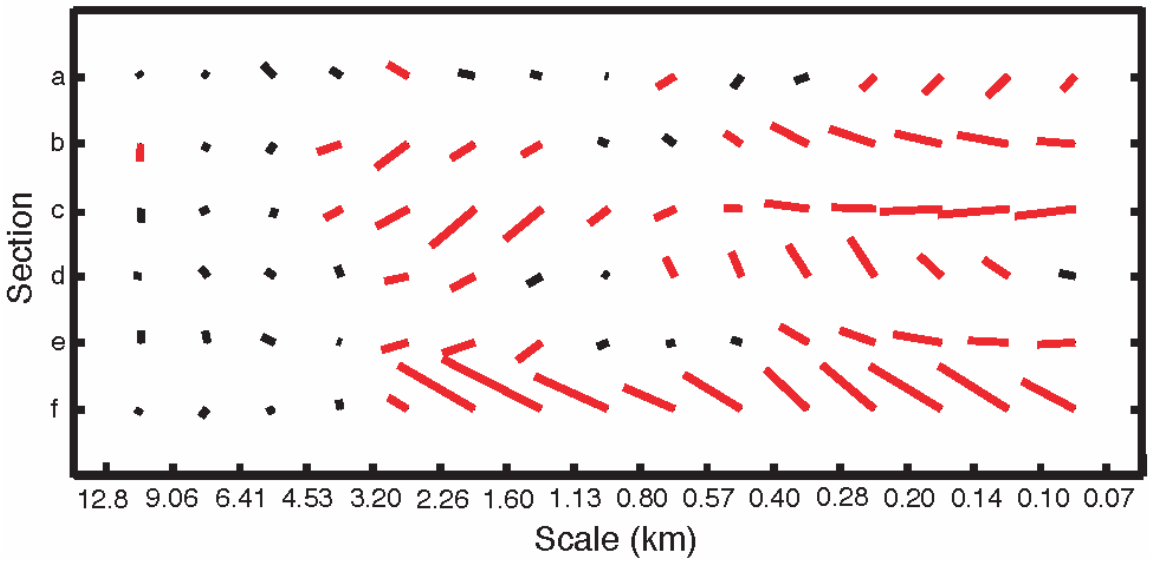

Figure 11. Anisotropy parameter vectors for the eight regions marked in Figure 10.

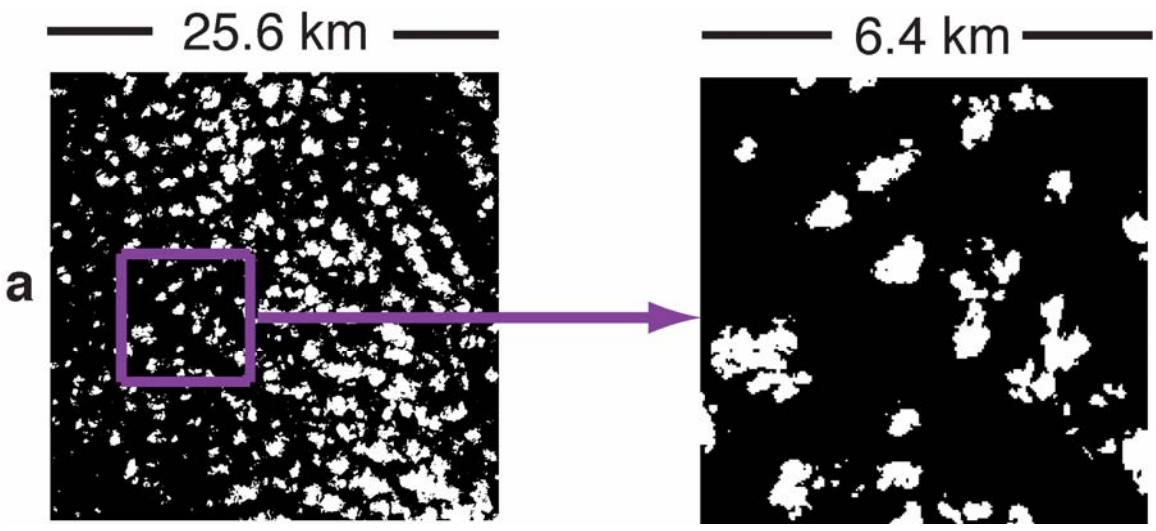

Figure 12. Enlargements of the cloud mask for region a in Figure 10. Again, individual cloud elements are oriented perpendicular to the large-scale (cloud street) axis. The large-scale anisotropy is especially strong in this case.

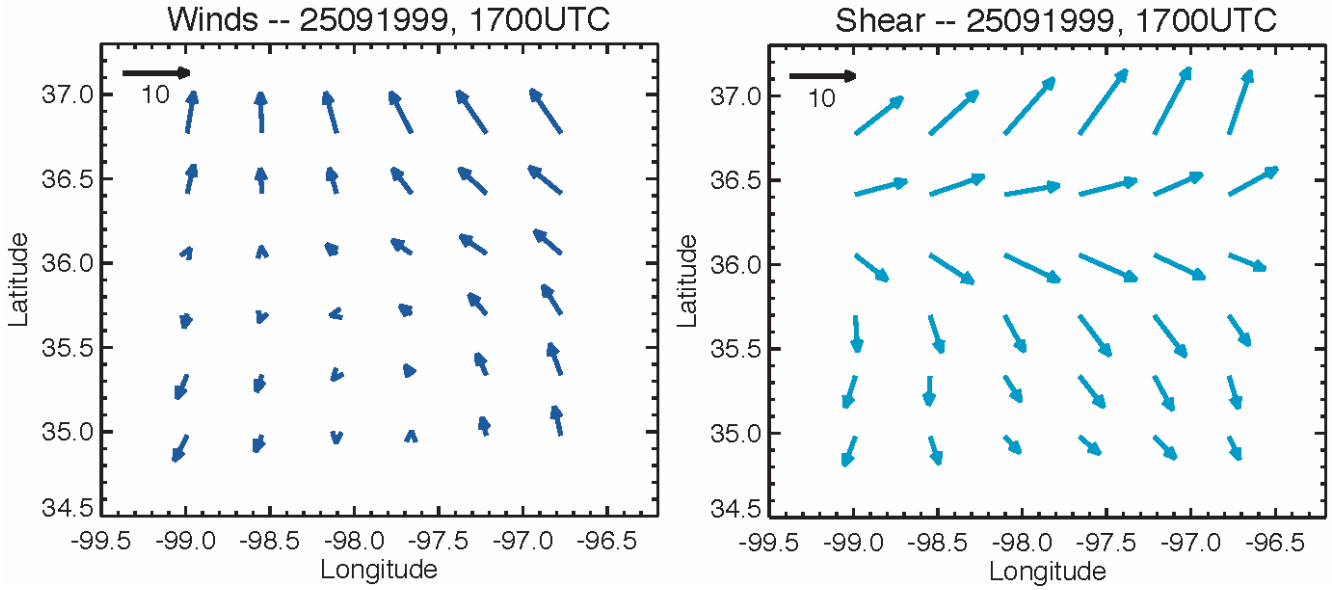

Figure 13. Wind and shear fields for the entire Landsat scene at 1700 UTC on June 29, 2002.

July 15, 2002 (Figures 14 to 17)

These fair-weather cumulus clouds are expected to be nearly isotropic, yet SW-NE alignment is found consistently at small scales, and weak alignment is even found in some cases at large scales. The orientation of large-scale features is near the mean wind direction, but small-scale anisotropy is detected nearly perpendicular to the mean shear. However, correlation with shear is extremely difficult because the shear direction and magnitude fluctuate rapidly with location.

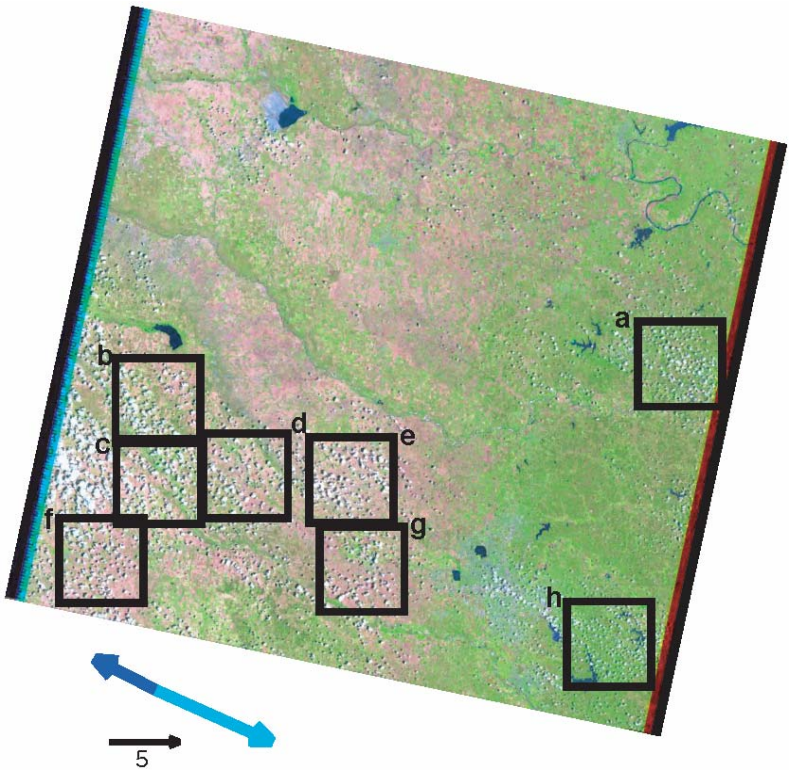

Figure 14. False-color Landsat ETM scene over central Oklahoma for July 15, 2002, showing fair-weather cumulus clouds.

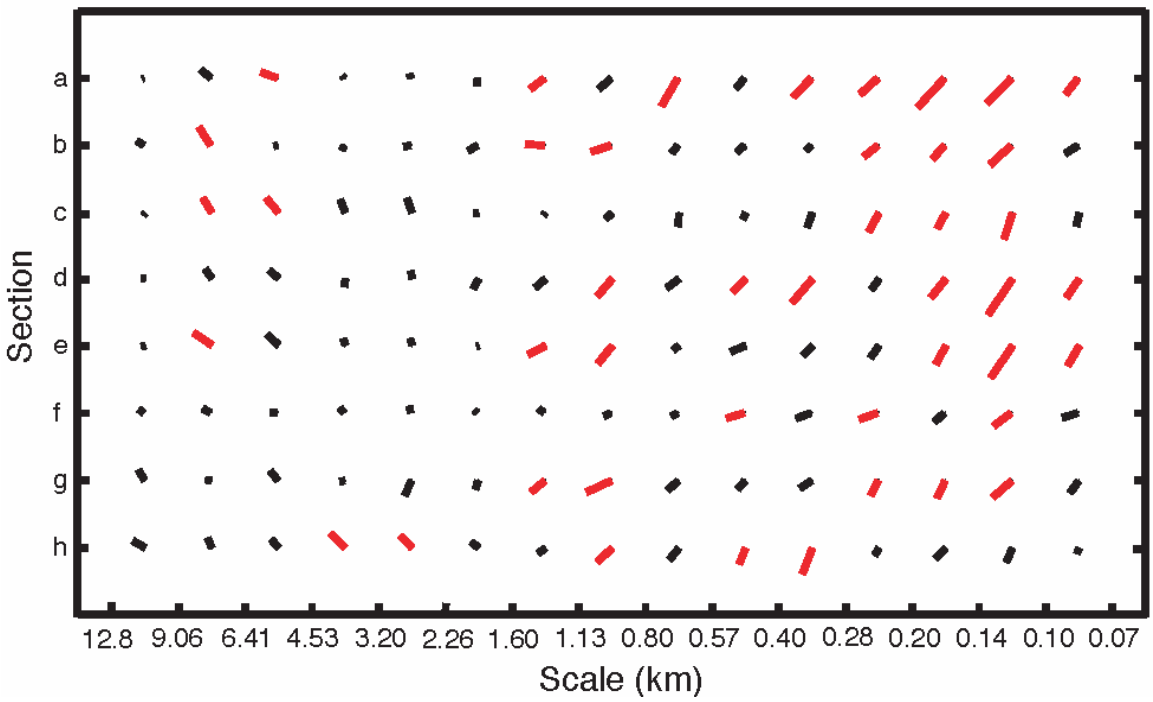

Figure 15. Anisotropy parameter vectors for the eight regions marked in Figure 14.

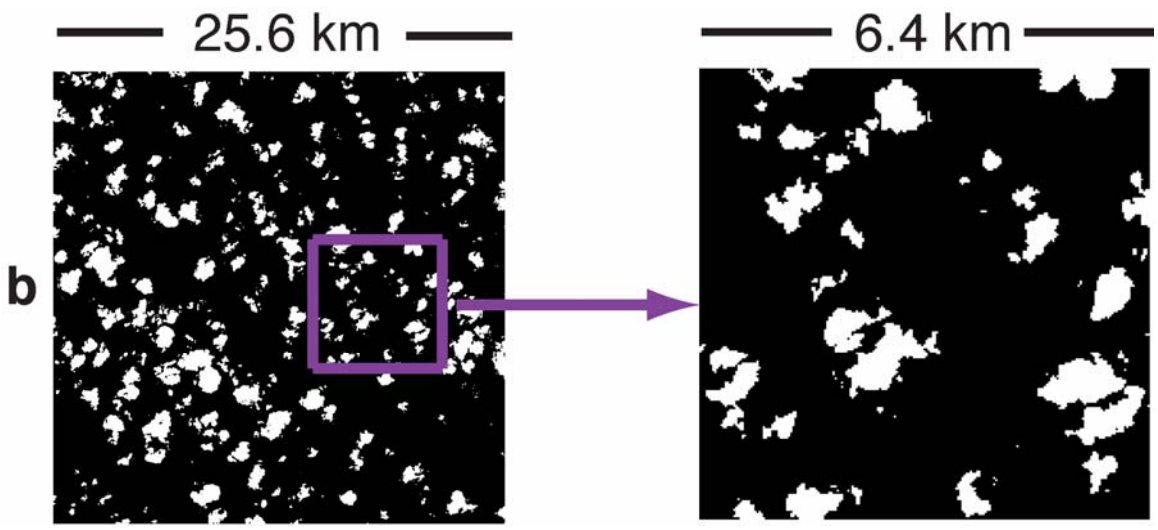

Figure 16. Enlargements of the cloud mask for region b in Figure 14. Although the anisotropy evident at all scales is weak, the large and small scale orientations are again nearly perpendicular.

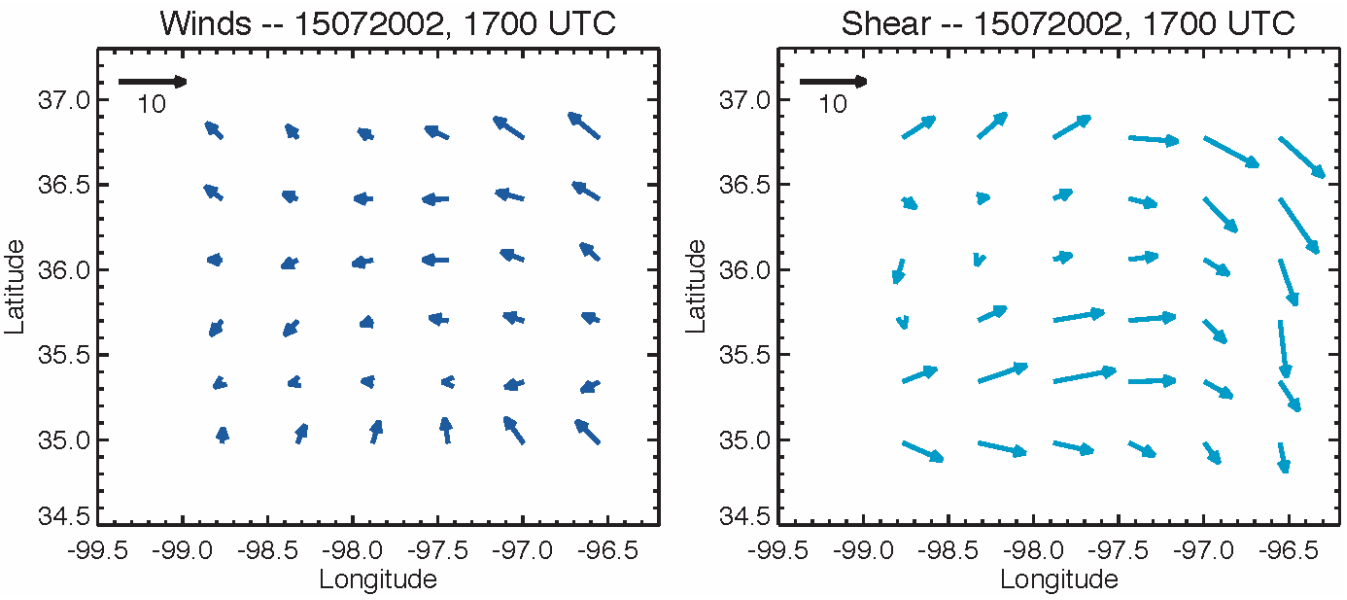

Figure 17. Wind and shear fields for the entire Landsat scene at 1700 UTC on July 15, 2002.

Conclusions

The anisotropy vectors computed match the cloud features apparent in the images. This is particularly obvious in the case of mesoscale structures.

Cloud field anisotropy amplitude and direction can vary significantly over the scale of Landsat images (~200 km). This occurs when the wind field varies over the area.

The strength and direction of cloud field orientation often vary with scale. Frequently the larger scales (>2 km) are aligned close to the direction of the wind while the smaller scales align parallel to the shear. This suggests that different mechanisms are responsible for organizing cloud fields at different scales.

Correlation of computed anisotropy and wind fields is complicated by variations in the winds over time and space. The satellite images correspond to an instant in time while the RUC dynamic fields incorporate a variety of data types and sources. In any case, analysis of many more scenes would be required to draw broader conclusions about the range and causes of anisotropy that occurs in broken cloud fields. It would be useful to improve the strategy used in comparing anisotropy and meteorological fields before undertaking such a study.

Corresponding Author

Laura Hinkelman, laura@nianet.org, (757) 864-5399

References

Hinkelman, L. M., K. F. Evans, E. E. Clothiaux, and T. P. Ackerman, 2002: The effect of fair-weather cumulus cloud field anisotropy on radiative surface fluxes. In *Proceedings of the Twelfth Atmospheric Radiation Measurement (ARM) Science Team Meeting*, ARM-CONF-2002. U.S. Department of Energy, Washington, D.C. Available URL: http://www.arm.gov/publications/proceedings/conf12/extended_abs/hinkelman-lm.pdf

Hinkelman, L. M., B. Stevens, and K. F. Evans, 2004: A Large-Eddy Simulation Study of Anisotropy in Fair-Weather Cumulus Cloud Fields. *JAS*, submitted.